

# Characterization of Time Delay Interferometry combinations for the LISA instrument noise

Olaf Hartwig\*

*Max-Planck-Institut für Gravitationsphysik (Albert-Einstein-Institut),  
Callinstraße 38, 30167 Hannover, Germany*

Martina Muratore†

*Dipartimento di Fisica, Università di Trento and Trento Institute for  
Fundamental Physics and Application / INFN, 38123 Povo, Trento, Italy*

(Dated: May 16, 2020)

## Abstract

Time delay interferometry (TDI) is a post-processing technique used in the Laser Interferometer Space Antenna (LISA) to reduce laser frequency noise by building an equal-arm interferometer via combining time-shifted raw phase measurements. Many so-called 2nd generation TDI variables have been found that sufficiently suppress laser frequency noise considering realistic LISA orbital dynamics.

In this paper, we want to investigate the relationships between these different TDI channels to understand the optimal approach for recovering all information from the raw phase measurements. It is already well known from the literature that the entire space of TDI solutions can be generated out of the 4 combinations  $\alpha$ ,  $\beta$ ,  $\gamma$ , and  $\zeta$ , at least under the approximation of three different but constant constellation arms (1st generation TDI). We apply this result to a core subset of the 2nd generation combinations reported in the literature, for which we compute explicitly how they can be approximated in terms of these 4 generators and show numerically that these approximations are accurate enough to model the noises not suppressed by TDI. Finally, we identify multiple possible 2nd generation representatives of  $\alpha$ ,  $\beta$ ,  $\gamma$ , and  $\zeta$ , and discuss which might be ideal to use for the LISA data analysis. In addition, we demonstrate that newly found variants of the variable  $\zeta$  significantly out-perform the ones previously known from the literature.

---

\* contact: olaf.hartwig@aei.mpg.de

† contact: martina.muratore@unitn.it

## 1. INTRODUCTION

Gravitational waves (GWs) are predicted by General Relativity and were first observed in 2016 by the two ground-based interferometers LIGO [1]. They can be detected by laser interferometers which recover the Doppler shift that a passing GW causes on the frequency of the laser beam.

The Laser Interferometer Space Antenna (LISA), which is the 3rd large mission (L3) of the ESA program Cosmic Vision has the goal of detecting gravitational waves with frequencies in the mHz regime by tracking the relative distance between two free-falling test masses (TMs), hosted in distant spacecraft, using laser interferometry [2].

The constellation is designed to have three identical spacecraft in a triangular formation which are separated by 2.5 million km, with six active laser links connecting them. The orbits are chosen to have a constellation forming a triangle as equilateral as possible. However, due to celestial dynamics, the arms differ from each other by  $\pm 1\%$  and the satellites have a relative drift of up to  $10 \text{ m s}^{-1}$ . As a consequence, the LISA interferometers will have unequal and time-varying arm-lengths, such that they will be strongly affected by laser frequency noise. Thus, to compensate for this noise we apply a post-processing technique called time-delay interferometry (TDI). This post-processing technique combines on ground the raw phase meter data by properly time-shifting them in order to build an equivalent equal arm interferometer, insensitive to laser frequency noise. Many such data combinations are possible, such as the Michelson-like interferometer  $X$  or the Sagnac combination  $\alpha$  [3].

One approach to find TDI data combinations is geometric TDI, first introduced in [4]. This approach was recently revisited in [5], where new combinations of signals which fulfil the frequency noise suppression requirements were found. In particular, [5] reports 174 combinations of 16-links and 12 of 12-links while in [4], only 48 of 16-links and none of 12-links were advertised<sup>1</sup>. These combinations could be reduced to a subset of 35 of 16-links and 3 of 12-links, if one considers as equal combinations that differ by any permutation of the satellites.

Moreover, additional combinations of 14-links that were missing in the previous catalogue are reported in [6], where it is illustrated that the total number of combinations could be

<sup>1</sup> We call a 'link' the one-way Doppler measurement between two of the LISA spacecraft. Note that [4] also includes solutions of up to 24 links, which were not investigated in [5].

reduce to a subset of 28 of 16-links, 3 of 14-links and 3 of 12-links, if one considers as equal combinations that differ only by any permutations of satellites or a time reversal symmetry. Including these symmetries, the set grows to a total of 210 distinct combinations up to 16 links.

On the other hand, the space of possible TDI solutions can also be described and constructed algebraically, at least under certain assumptions [7]. It turns out that the entire space of 1st generation TDI (three unequal and constant interferometer arms) can be generated out of 4 combinations [8], while for 1.5th generation TDI variables, 6 fundamental variables are needed [9]. Conversely, the general algebraic problem of second generation TDI (meaning linearly evolving arms) is up to date still unsolved [7].

Lacking a theorem guaranteeing that all 2nd generation variables can be constructed from a finite set of generators, the question arises if some of the 210 combinations contain redundant information and if we are able to find a minimum set of TDI variables containing all the relevant information we need to perform the LISA data analysis. To this end, we remark that for the purpose of estimating the coupling of non-suppressed effects, like gravitational waves and most secondary noise sources<sup>2</sup>, it is usually sufficient to study TDI under the assumption of 1st generation TDI. The reason is that while small mismatches and dynamic changes in the armlengths have to be taken into account when we aim to reduce laser frequency noise (by several orders of magnitude) they only cause very small corrections to the expressions for the non-suppressed effects.

Although it is often considered sufficient to use '0th generation' TDI (meaning three constant and equal arms) to perform data analysis, recent studies showed that neglecting the percent level static arm-length mismatches can in some cases bring large errors when modelling the instrument response to non-suppressed noises and GW signals [6]. On the other hand, considering three unequal arms was sufficient there to accurately predict the result of numerical simulations performed taking the full orbital dynamics into account.

In the rest of the paper, we do a follow up of [6], studying algebraic relationships between the new TDI combinations presented there under the same assumption of 1st generation

---

<sup>2</sup> Secondary noises such as test mass and readout noise are not suppressed in the output of TDI combinations, but only modulated by differences of the large delays applied when constructing the combination.

TDI to investigate which TDI channels should be suggested for the LISA data analysis. The rest of the article is divided in three sections. In section 2, we report the core combinations found in [6] and we illustrate how we can highlight similarities between them by simplifying these combinations under the assumptions of 1st generation TDI. Moreover, we compute explicitly how each of these simplified combinations is related to the four generators of first generation TDI,  $\alpha$ ,  $\beta$ ,  $\gamma$  and  $\zeta$ , and discuss the implications for LISA data analysis. We then demonstrate numerically in section 3.1 that the decompositions of 2nd generation variables into the 1st generation generators are good approximations for the secondary noises. We run simulations without laser frequency noise, which allows us to compute the first generation variables, whereas we keep readout noise and test-mass acceleration noise enabled. These simulations show that the approximations are valid to within 3 to 5 orders of magnitude, depending on the Fourier frequency and TDI variable considered. We also discuss pros and cons of different sets of second generation variables that we can use to represent the first generation generators  $\alpha$ ,  $\beta$ ,  $\gamma$  and  $\zeta$ .

Moreover, we demonstrate numerically in section 3.2 that the previously described approximations remain valid also in the presence of laser noise. We show that a set of four 2nd generation combinations can be used to generate the instrument noise response of the channel X as an example, with a relative error of less than  $\approx 10^{-2}$  to  $10^{-5}$ , again depending on the Fourier frequency considered.

In addition, we analyse the laser noise suppression capabilities of the second generation  $\zeta$  variables given in [7] with respect to the new second generation  $\zeta$  variables found in [6]. The latter show to suppress laser noise several orders of magnitude more than the former and far below the level of secondary noises. Conversely, the residual laser noise of the previously known  $\zeta$  variable would present a significant noise contribution to the full LISA noise budget.

Finally, we report our conclusion and future perspective in section 4.

## 2. GENERATORS OF FIRST GENERATION TDI AND APPLICATION TO GEOMETRIC TDI

The formalism of geometric TDI [4, 5] allows to understand physically the properties of TDI combinations, and more practically, enables a systematic search for 2nd generation TDI

combinations.

We report in table I the list of the 34 core combinations<sup>3</sup> found in [6]. We express them in terms of time shifts applied to the intermediary TDI variables  $\eta_{ij}$ , using the notation described in appendix A.

The  $\eta_{ij}$  are constructed in post-processing from the raw measurements provided by the spacecraft, and correspond to direct tracking of the distance between the two TMs in a LISA link [11]. These virtual measurements contain the difference between the laser frequency fluctuations  $\phi_i$  and  $\phi_j$  of the local and received laser beams, respectively, where the received beam enters with a time delay by the light travel time  $d_{ij}(\tau)$ :

$$\eta_{ij}(\tau) = \phi_j(\tau - d_{ij}(\tau)) - \phi_i(\tau) + N_{ij}(\tau). \quad (1)$$

While the laser noise terms  $\phi_j$  and  $\phi_i$  will be strongly suppressed in post-processing, the  $N_{ij}$  term summarises any effects not fully suppressed by TDI. In particular,  $N_{ij}$  contains unavoidable secondary noises, such as acceleration noise of the TMs and noise introduced by the optical metrology system, as well as gravitational waves. Note that this is a simplified model for the LISA measurements, see e.g. [11] for a more detailed description.

We now want to study how these non-suppressed effects appear in the 34 core TDI combinations, and how many of these combinations we need to extract all information contained in our raw measurements. To this end, we want to express all variables in terms of a finite set of generators. As we introduced, the algebraic problem of second generation TDI is to date still unsolved [7], such that no set of generators is known for this case. Instead, we study these TDI combinations under the assumptions of first generation TDI since, as already proposed in [7] and empirically demonstrated in [6], this is sufficient to describe the instrumental noise and GW signal response. It is important to stress that in practice, we cannot use first generation TDI variables in the actual data analysis, since they don't suppress the laser noise sufficiently.

To avoid confusion, we will use a different notation for the six non-commutative delay operators of second generation, as used in table I, and the three commutative delay operators

---

<sup>3</sup> Note that these 34 core combinations can be used to generate all 210 variables presented as supplementary material in [6] by applying the appropriate symmetries and index permutations [10, 11]. In particular, the core combinations  $C_1^{16}, C_4^{16}, C_5^{16}, C_6^{16}, C_7^{16}, C_8^{16}, C_{21}^{16}$  and  $C_{22}^{16}$  can be used to generate all 48 variables presented in [4].

of first generation TDI. For the latter, we take inspiration from the literature, e.g. [7], and will denote the operators applying the corresponding delays by  $x$ ,  $y$  and  $z$ . They act on any time dependent function  $f(t)$  via

$$xf(t) = f(t - x^d), \quad yf(t) = f(t - y^d) \quad \text{and} \quad zf(t) = f(t - z^d), \quad (2)$$

where we compute the delays as

$$x^d = \text{mean} \left[ \frac{d_{23}(t) + d_{32}(t)}{2} \right] \quad (3a)$$

$$y^d = \text{mean} \left[ \frac{d_{31}(t) + d_{13}(t)}{2} \right] \quad (3b)$$

$$z^d = \text{mean} \left[ \frac{d_{12}(t) + d_{21}(t)}{2} \right], \quad (3c)$$

with  $d_{ij}(t)$  as the time series of time varying delays estimated from the orbits for a photon received on spacecraft  $i$  and emitted from spacecraft  $j$ . Since we have three satellites,  $i$  and  $j$  can take the values 1, 2 or 3, with  $i \neq j$ . Then  $\text{mean}[\dots]$  denotes a time average over the timespan of interest (usually a couple of hours), such that  $x^d$ ,  $y^d$  and  $z^d$  are indeed constants.

The corresponding advancements are denoted by  $x^{-1}$ ,  $y^{-1}$  and  $z^{-1}$ , and act as

$$x^{-1}f(t) = f(t + x^d), \quad y^{-1}f(t) = f(t + y^d) \quad \text{and} \quad z^{-1}f(t) = f(t + z^d). \quad (4)$$

We can map all second-generation variables presented in table I to first generation variables by replacing

$$\mathbf{D}_{12} = \mathbf{D}_{21} = z, \quad \mathbf{D}_{23} = \mathbf{D}_{32} = x, \quad \mathbf{D}_{31} = \mathbf{D}_{13} = y, \quad (5a)$$

$$\mathbf{A}_{12} = \mathbf{A}_{21} = z^{-1}, \quad \mathbf{A}_{23} = \mathbf{A}_{32} = x^{-1}, \quad \mathbf{A}_{31} = \mathbf{A}_{13} = y^{-1}. \quad (5b)$$

As known from the literature, see e.g., [7], one important result for 1st generation TDI is that all TDI variables can be constructed from just four generators. One possible set of generators are the 3 Sagnac variables  $\alpha$ ,  $\beta$ ,  $\gamma$  together with the fully symmetric Sagnac  $\zeta$

[3]. These are given in our notation as:

$$\alpha = \eta_{12} + z\eta_{23} + zx\eta_{31} - \eta_{13} - y\eta_{32} - yz\eta_{21} \quad (6a)$$

$$\beta = \eta_{23} + x\eta_{31} + xy\eta_{12} - \eta_{21} - z\eta_{13} - zy\eta_{32} \quad (6b)$$

$$\gamma = \eta_{31} + y\eta_{12} + yz\eta_{23} - \eta_{32} - x\eta_{21} - xz\eta_{13} \quad (6c)$$

$$\zeta = x\eta_{12} + y\eta_{23} + z\eta_{31} - x\eta_{13} - z\eta_{32} - y\eta_{21}. \quad (6d)$$

In the interpretation of geometric TDI,  $\alpha$ ,  $\beta$  and  $\gamma$  are simple two-beam interferometers, while  $\zeta$  is a 6 beam interferometer, where each spacecraft emits and receives two beams.

Following [7], we are therefore able to write each first generation TDI combination as

$$\text{TDI}_k = A'_k\alpha + B'_k\beta + C'_k\gamma + D'_k\zeta, \quad (7)$$

where  $\text{TDI}_k$  is the  $k$ 'th combination in table I after simplifying it using eqs. (5a) and (5b), while  $A'_k, B'_k, C'_k, D'_k$  are polynomials of the delay operators  $x, y$  and  $z$ . This means that under the assumptions of first generation TDI, all information we can extract from any of the combinations given in table I is, in principle, already contained in these four generators  $\alpha, \beta, \gamma$  and  $\zeta$ .

Note that solutions to eq. (7) are not necessarily unique, since  $\alpha, \beta, \gamma$  and  $\zeta$  have a time-delay relationship to each other [7]:

$$(1 - xyz)\zeta = (x - yz)\alpha + (y - xz)\beta + (z - xy)\gamma. \quad (8)$$

As argued in [7], the term  $(1 - xyz)$  appearing in front of  $\zeta$  in this equation theoretically does not impact the signal to noise ratio, such that one could consider just  $\alpha, \beta$  and  $\gamma$  for the astrophysical data analysis. However, we will argue in section 3.1 that terms like this  $(1 - xyz)$  can have subtle impacts on the data analysis, such that we consider all four generators for our analysis.  $\zeta$  in particular is known to be insensitive to GWs at low frequencies, and is therefore of interest for characterizing the instrument [3].

Before explicitly solving eq. (7) for all core variables, we further simplify the expressions by applying an overall time shift<sup>4</sup>  $E_k$  to each expression given in table I, such that we solve

<sup>4</sup> We determine  $E_k$  by collecting the common factors in front of each  $\eta_{ij}$  in table I after we used eqs. (5a) and (5b) to simplify the combinations from 2nd to 1st generation TDI.

the following equation instead of eq. (7):

$$E_k \text{ TDI}_k = A_k \alpha + B_k \beta + C_k \gamma + D_k \zeta. \quad (9)$$

We solve eq. (9) for each value of  $k$  using the computer software `Mathematica`. Since each of the six  $\eta_{ij}$  is independent, eq. (9) can be read as a system of six linear equations, which we first solve for four real coefficients  $A_k$ ,  $B_k$ ,  $C_k$  and  $D_k$ . Note that the actual solutions to eq. (9) are only those for which  $A_k$ ,  $B_k$ ,  $C_k$  and  $D_k$  are also valid polynomials in  $x$ ,  $y$  and  $z$ . In particular, we must not allow solutions containing the inverse of a multi term polynomial such as, e.g.,  $1/(x - yz)$ .

We describe in appendix C how to retrieve the equivalent expressions for the remaining 174 combinations of the full set of TDI variables from these core combinations.

## 2.1. Discussion

Many of the variables are given as one of the generators  $\alpha$ ,  $\beta$ ,  $\gamma$  or  $\zeta$  with a single difference of delays in front (e.g.,  $C_1^{12} \approx (1 - xyz)\alpha$  and  $C_{28}^{16} \approx (y^2 - z^2)\zeta$ ). This implies that there are multiple choices of second generation representatives of the first generation generators given in eq. (6a) to eq. (6d). Indeed, each of these representatives response to GWs and noise can be computed by applying different frequency domain transfer functions to the response of the first generation variables. As argued in [7], these transfer functions do not impact the SNR in theory, such that any of them could be used in the data analysis. However, since in practice TDI variables are computed numerically with finite dynamic range and sampling rate, some variables might have better SNR around some singular frequencies, and might also have other advantages. We will discuss some of these points in section 3.1.

In addition, we observe that  $C_4^{16}$ ,  $C_{24}^{16}$  and  $C_{28}^{16}$  contain an overall difference term  $(y - z)$  or  $(y^2 - z^2)$ . These terms are vanishing if all delays are assumed equal (i.e., assume  $x = y = z$ ) as explicitly shown for the '0th generation' expressions in table II. This means that when we take the real LISA orbital dynamics into account, the secondary noises as well as the astrophysical signal will be strongly suppressed in these variables. However, they are not



exactly vanishing, which highlights that the assumption of equal arms is not sufficient to accurately model the response of some variables.

Furthermore, since the  $\zeta$  combinations has the special properties of being less sensitive to gravitational waves compared to  $\alpha$ ,  $\beta$  and  $\gamma$ , at least at low frequencies, we would expect this property to extend to  $C_3^{12}$ ,  $C_3^{14}$ ,  $C_{26}^{16}$ ,  $C_{27}^{16}$  and  $C_{28}^{16}$ , which are directly related to the first generation  $\zeta$ . This could make these variables useful for characterising the instrumental noise in the presence of a GW signal, and to distinguish a stochastic GW background from the noise, as discussed in [6]. Note that, as shown in fig. 4, these combinations suppress laser noise to the same level as all other variables, contrary to the second generation version of  $\zeta$  proposed in [7].

### 3. NUMERICAL SIMULATIONS

We run two simulations using `LISA Instrument`<sup>5</sup> to verify our statement that the decompositions shown in table II are good approximations for the secondary noises. In both simulations, all noise time series are generated at a high sampling rate of 16 Hz and then filtered and decimated to a lower measurement rate of 4 Hz. The filter is a digital symmetrical FIR filter build from a Kaiser windowing function, with a transition band extending from 1.1 Hz to 2.9 Hz and a minimum attenuation above 2.9 Hz of 320 dB.

In the first simulation, we disable laser noise, which allows us to use the first generation generators  $\alpha$ ,  $\beta$ ,  $\gamma$  and  $\zeta$ . We simulate readout noise and test-mass acceleration noise, as they are the main noise contributors of the instrumental noise after TDI, and use realistic orbits provided by ESA to compute the light travel times. This allows us to directly test the validity of the decomposition given in table II for all the combinations.

In the second set of simulations, we simulate laser noise as well, such that we are restricted to use only the second generation variables. We then show that the relationships given in table II remain valid by constructing a version of  $C_1^{16}$  out of  $C_{27}^{16}$  and the three cyclic permutations of  $C_1^{12}$ .

---

<sup>5</sup> `LISA Instrument` is a time-domain LISA simulator developed by J.-B. Bayle inside the LISA Consortium. See [11, 13?] for a detailed description of its simulation model.

All TDI combination are computed using PyTDI<sup>6</sup>.

### 3.1. Simulations without laser noise

We simulate  $10^5$  samples of LISA data with the aforementioned parameters, and compute the response of all TDI combinations given in table I. Here, we use the time-varying light travel times  $d_{ij}(t)$  output by the simulation to compute the exact response of the variable given realistic orbits.

We then compute the constant delays  $x^d$ ,  $y^d$  and  $z^d$  using eqs. (3a) to (3c), and use them to construct the generators of first generation TDI as given in section 2. This allows us to use the expressions given in table II to construct the approximate versions of all TDI combinations. We can then study the time-domain residual between the exact and approximate version of each variable.

As an example, we plot in fig. 1 the amplitude spectral density (ASD) of the TDI combinations  $C_1^{12}$ ,  $C_3^{12}$ ,  $C_1^{14}$ ,  $C_1^{16}$ , and  $C_{24}^{16}$  as given in table I. In addition, we also plot the ASD of the time-domain residual between them and their expressions in terms of  $\alpha$ ,  $\beta$ ,  $\gamma$  and  $\zeta$  from table II. We observe that the residuals for all variables are at a similar level, about four to five orders of magnitude below the actual secondary noise levels of  $C_1^{12}$ ,  $C_3^{12}$ ,  $C_1^{14}$  and  $C_1^{16}$ , such that the expressions given in table II should provide good approximations of the secondary noises.

Looking at the plot, we see that the combinations show to have different noise shapes, in particular, their spectra have an unequal number of zeros. This can be explained by referring to the column of table II which shows the approximation in case of equal arms ('0th' generation). We see that all variables contain a difference term of the form  $(1 - D^N)$ , where  $D$  is the single delay operator of '0th' generation TDI, acting as  $Df(t) = f(t - \bar{d})$ , with  $\bar{d} \approx 8.3$ s as the arm length. In the frequency domain, this term corresponds to a transfer function of the form  $2 \left| \sin(\pi f N \bar{d}) \right|$ , with zeros at frequencies  $f = (N\bar{d})^{-1}$ .

For example,  $C_1^{16}$  has  $N = 4$ , thus shows to have zeros starting at  $f \approx 30$  mHz. It is then followed by  $C_1^{12}$  with  $N = 3$ ,  $C_1^{14}$  with  $N = 2$  and  $C_3^{12}$  with  $N = 1$ .

---

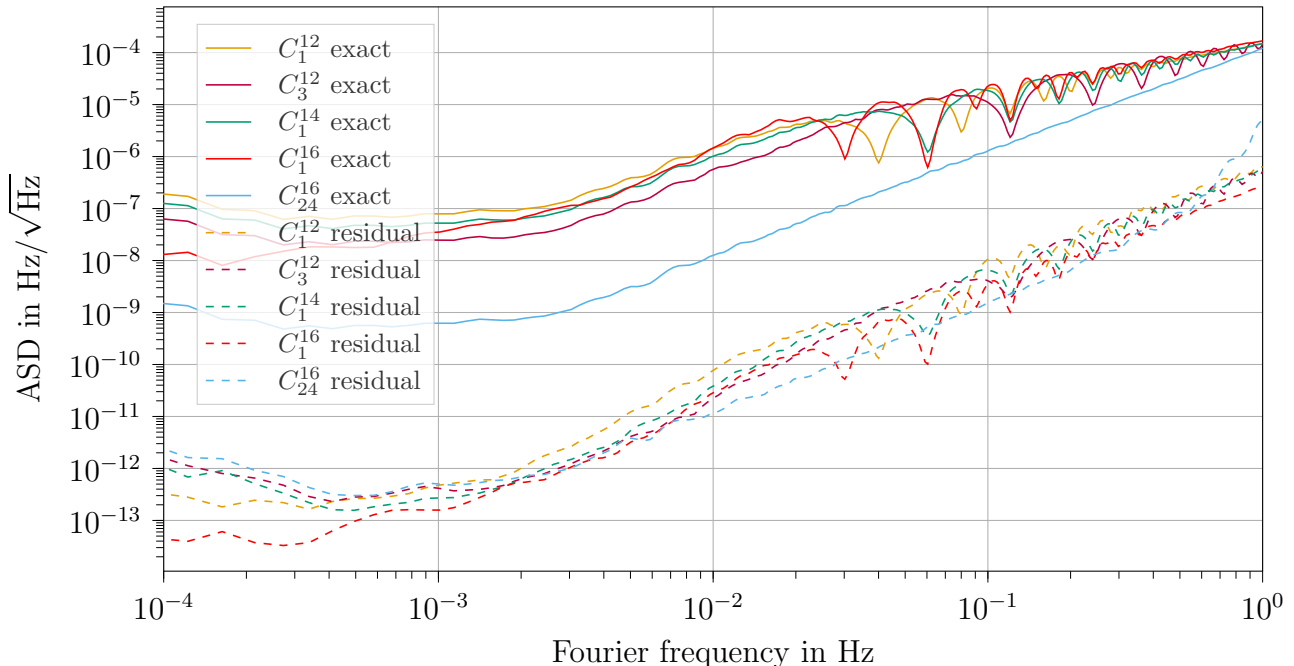
<sup>6</sup> PyTDI is a python package designed to compute TDI combinations, developed mainly by M. Staab and J.-B. Bayle inside the LISA consortium.

$C_{24}^{16}$  behaves differently, since it is exactly vanishing when assuming equal arms. However, it is not vanishing in the assumption of 1st generation TDI, where it contains a difference term  $z^2 - y^2$ . This corresponds to a frequency domain transfer function of  $2\left|\sin(2\pi f(z^d - y^d))\right|$ , which has zeros outside of the LISA band, at  $f = 0.5(z^d - y^d)^{-1} \approx 5$  Hz. This explains why the blue curve describing  $C_{24}^{16}$  in fig. 1 appears at a lower level than those of  $C_1^{12}$ ,  $C_3^{12}$ ,  $C_1^{14}$  and  $C_1^{16}$ , since the transfer function starts suppressing the output for frequencies below 5 Hz, whereas for the others, the roll-off starts only around  $5 \times 10^{-2}$  Hz. Note that this lower noise level might imply that this variable is more susceptible to errors due to the finite numerical precision of our data.

On the other hand, as already argued in [4], zeros inside the LISA band can also negatively impact the data analysis, even though they affect both signal and noise equally. Indeed, while the signal to noise ratio is theoretically unchanged, in practice, our data has finite dynamic range, such that the zeros are 'filled' by numerical noise, causing a degradation of SNR close to the zeros. It is therefore potentially beneficial to use TDI combinations with as few zeros as possible.

We now want to compare different possible 2nd generation versions of the generator  $\alpha$ . As argued above, these differ by the differential time delays applied to them, which correspond to frequency domain transfer functions of the form  $2\left|\sin(\pi f \delta)\right|$ , with  $\delta$  as the differences of the applied delays. At low frequencies, we can expand this transfer function to first order in  $\delta$ , to get a simple factor  $2\pi f \delta$ , which represents a derivative combined with a rescaling by  $\delta$ . Thus, it is interesting to compare the different possible second generation versions of  $\alpha$  to the derivative of the first generation version. We plot in fig. 2 the combinations  $C_1^{12}$ ,  $C_2^{12}$ ,  $C_1^{14}$ ,  $C_3^{16}$  and  $C_{24}^{16}$ , all rescaled by their respective  $\delta$ , compared to the two-point derivative of  $\alpha$  (labelled  $\dot{\alpha}$ ). We observe that as expected, all curves coincide at low frequencies, while the different number of zeros determines the deviations at high frequencies. In particular, we observe that  $C_{24}^{16}$  seems to approximate  $\dot{\alpha}$  very well across the whole frequency band. However, even if fig. 1 shows that the approximation reported in table II holds within 3 orders of magnitude, we are not able to demonstrate that  $C_{24}^{16}$  agrees to  $\dot{\alpha}$  to this precision. The reason is that the two-point derivative we used to compute  $\dot{\alpha}$  has a time difference of  $1/f_s = 0.25$  s, that is different to the one of  $C_{24}^{16}$ , which is  $2(z^d - y^d) \approx 0.2$  s. We discuss this

FIG. 1. Secondary noises in  $C_1^{12}$ ,  $C_3^{12}$ ,  $C_1^{14}$ ,  $C_1^{16}$  and  $C_{24}^{16}$  compared to the residual between the approximation given in table II and their exact expression given in table I.

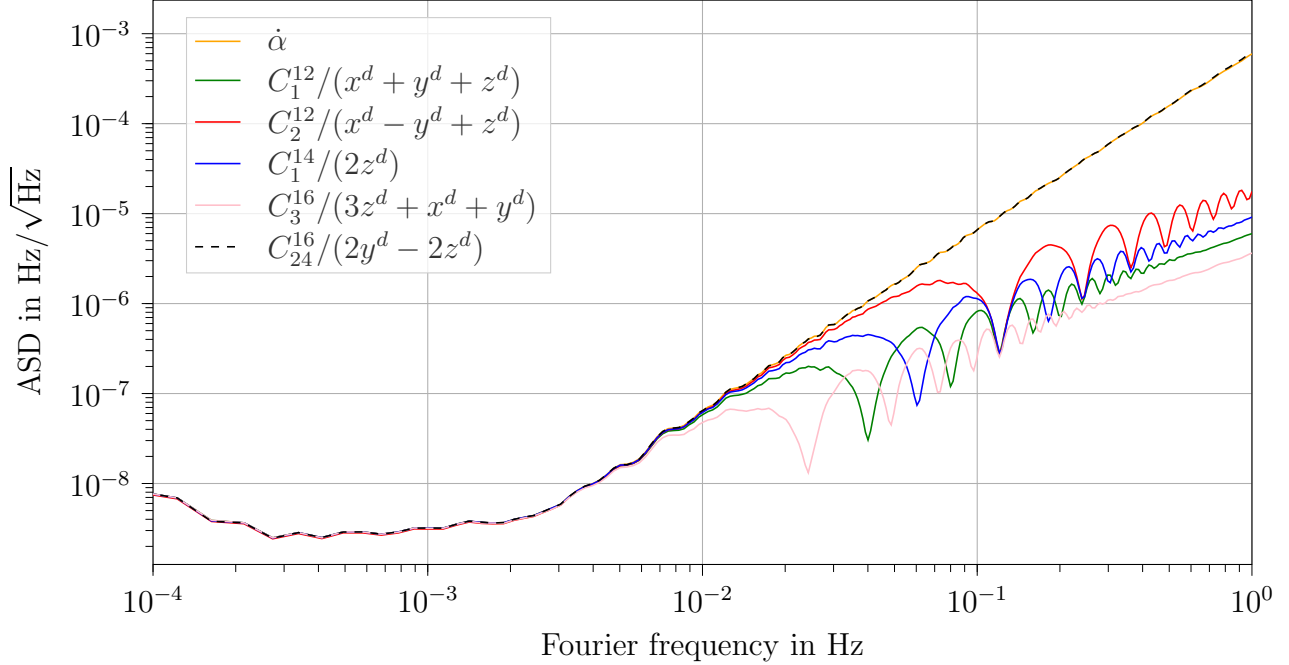


in detail in appendix B.

As a proof of concept that the decompositions presented in table II are still applicable when we include laser noise in the simulation, we want to linearly combine multiple second generation variables to construct the variable  $C_1^{16}$  (known in the literature as TDI X). The previously discussed set of variables without zeros in the LISA band seem to be good candidates to use in this construction. However, we remark that the two cyclic permutations of  $C_{24}^{16}$  contain the time differences  $2(x^d - z^d)$  and  $2(y^d - z^d)$ , respectively, such that including  $C_{24}^{16}$  itself, we get finite difference approximations of  $\dot{\alpha}$ ,  $\dot{\beta}$  and  $\dot{\gamma}$  with unequal time differences. The same argument holds for  $C_{28}^{16}$ , which approximates  $\dot{\zeta}$ . This limits our ability in using linear combinations of these variables to build other variables in the table, as discussed in appendix B and illustrated in fig. 6.

On the other hand, as visible in table II, the variables  $C_1^{12}$  (plus its cyclic permutations  $\hat{C}_1^{12}$  and  $\hat{\hat{C}}_1^{12}$ ) and  $C_{27}^{16}$  all have the same time shift factor  $(1 - xyz)$  applied to them. This allows us to linearly combine them without introducing additional errors, as we demonstrate in the next section.

FIG. 2. Second generation variables as approximation of the derivative of  $\alpha$ .  $C_1^{12}$ ,  $C_2^{12}$ ,  $C_1^{14}$ ,  $C_3^{16}$  and  $C_{24}^{16}$  are rescaled by the numerical value of the difference of delays applied in table II. Combinations with larger delay differences have more zeros inside the LISA band.



### 3.2. Simulations including laser noise

Let us define a short-hand notation for the second generation representatives of the variables  $\alpha$ ,  $\beta$ ,  $\gamma$  and  $\zeta$  chosen for this example:

$$\tilde{\alpha} \equiv C_1^{12} \quad (10a)$$

$$\tilde{\beta} \equiv \hat{C}_1^{12} \quad (10b)$$

$$\tilde{\gamma} \equiv \hat{\hat{C}}_1^{12} \quad (10c)$$

$$\tilde{\zeta} \equiv xC_{27}^{16}. \quad (10d)$$

Applying the factor  $(1 - xyz)$  to the expression given for  $C_1^{16}$  in table II, we see that

$$(1 - xyz)C_1^{16} \approx (1 - y^2z^2)(1 - xyz)(\alpha - z\beta - y\gamma + yz\zeta) \quad (11a)$$

$$\approx (1 - y^2z^2)\left(\tilde{\alpha} - z\tilde{\beta} - y\tilde{\gamma} + yz\tilde{\zeta}\right). \quad (11b)$$

To verify that eq. (11b) is accurate, we compute the exact version of  $C_1^{16}$  given in table I numerically, and apply the additional factor  $(1-xyz)$  to the resulting laser-noise free variable. We compare it to the approximated version on the right hand side of eq. (11b), where we compute  $\tilde{\alpha}$ ,  $\tilde{\beta}$ ,  $\tilde{\gamma}$  and  $\tilde{\zeta}$  as given in eqs. (10a) to (10d).

Figure 3 shows that the noise level of the simulated data (in orange) is well explained by the analytical model describing the secondary noises (in dotted grey). For clarity the approximated solution of  $(1-xyz)C_1^{16}$  is omitted as we cannot appreciate the difference with respect to the exact solution on this scale. We show instead that the residual noise between the left- and right-hand side of eq. (11b) is several orders of magnitude below the secondary noises. This same principle could easily be applied to any of the variables given in table II.

However, since all information is already contained in  $\alpha$ ,  $\beta$ ,  $\gamma$  and  $\zeta$ , it should be enough in practice to compute a single set of second generation versions of them, without a need to construct other variables (such as  $C_1^{16}$ ) out of them.

Note that the second generation versions of  $\zeta$  considered here, such as  $C_{27}^{16}$  or  $C_{28}^{16}$ , are different from the second generation  $\zeta$  proposed in [7]. Figure 4 compares the residual laser noise for the 1st and 2nd generation  $\zeta$  variable from the literature with that in  $C_{27}^{16}$  and  $C_{28}^{16}$ . For reference, we also p

lot a typical  $1 \text{ pm}/\sqrt{\text{Hz}}$  noise allocation<sup>7</sup>. We see that both  $C_{27}^{16}$  and  $C_{28}^{16}$  reduce laser noise far below the level of the previously known variables (and the requirements), as also demonstrated by theoretical calculation in [5].

---

<sup>7</sup> The overall noise allocation given for the interferometric readout given in [14] is  $10 \text{ pm}/\sqrt{\text{Hz}}$ . It is common to compare individual noise sources to a more conservative requirement, such that no single noise source uses up the whole allocated noise level. In addition, we applied the readout noise TDI transfer function for the second generation  $\zeta$  variable given in the literature [7]. Note that we omit the usual relaxation of the requirement towards low frequencies, to compensate for the fact that the simulation assumes laser frequency noise to be a white noise across the whole frequency band.



Name	Timeshift	Expression '1st' gen	Timeshift	Expression '0th' gen
$C_1^{12}$	1	$(1 - xyz)\alpha$	1	$(1 - D^3)\alpha$
$C_2^{12}$	$xy^2$	$(y - xz)\alpha$	$D^2$	$(1 - D)\alpha$
$C_3^{12}$	$yz$	$(y - xz)\zeta$	$D$	$(1 - D)\zeta$
$C_1^{14}$	$xy$	$(1 - z^2)\alpha$	$D^2$	$(1 - D^2)\alpha$
$C_2^{14}$	$yz$	$(1 - z^2)\gamma$	$D^2$	$(1 - D^2)\gamma$
$C_3^{14}$	$y$	$(1 - z^2)\zeta$	$D$	$(1 - D^2)\zeta$
$C_1^{16}$	1	$(1 - y^2z^2)(\alpha - z\beta - y\gamma + yz\zeta)$	1	$(1 - D^4)(\alpha - D\beta - D\gamma + D^2\zeta)$
$C_2^{16}$	1	$(1 - xyz^3)\alpha - z(1 - xyz)\beta$	1	$(1 - D^5)\alpha - (D - D^4)\beta$
$C_3^{16}$	1	$(1 - xyz^3)\alpha$	1	$(1 - D^5)\alpha$
$C_4^{16}$	$y^4z^2$	$(y^2 - z^2)(\alpha - z\beta - y\gamma + yz\zeta)$	$D^6$	0
$C_5^{16}$	$y^2$	$(1 - z^2)(\alpha - z\beta - y\gamma + yz\zeta)$	$D^2$	$(1 - D^2)(\alpha - D\beta - D\gamma + D^2\zeta)$
$C_6^{16}$	$xy$	$(1 - z^2)(z\alpha - \beta)$	$D^2$	$(1 - D^2)(D\alpha - \beta)$
$C_7^{16}$	$xy^3$	$(y - xz)(y\alpha - \gamma)$	$D^3$	$(1 - D)(D\alpha - \gamma)$
$C_8^{16}$	$y$	$(1 - xyz)(y\alpha - \gamma)$	$D$	$(1 - D^3)(D\alpha - \gamma)$
$C_9^{16}$	$x^2y^2z^2$	$(xy - z^3)\alpha + (z^2 - xyz)\beta$	$D^4$	$(1 - D)(\alpha + \beta)$
$C_{10}^{16}$	$x^2y$	$(x - yz^3)\alpha + (yz^2 - xz)\beta$	$D^2$	$(1 - D^3)\alpha + (D^2 - D)\beta$
$C_{11}^{16}$	$y$	$(1 - x^2z^2)\alpha$	$D$	$(1 - D^4)\alpha$
$C_{12}^{16}$	$y^2$	$(1 - xyz)\alpha + (xz - y)\gamma$	$D^2$	$(1 - D^3)\alpha + (D^2 - D)\gamma$
$C_{13}^{16}$	$x^2yz$	$(xy - z^3)\alpha$	$D^2$	$(1 - D)\alpha$
$C_{14}^{16}$	$y$	$(xyz^2 - z)\gamma + (1 - xyz^3)\zeta$	$D$	$(D^4 - D)\gamma + (1 - D^5)\zeta$
$C_{15}^{16}$	$xz^2$	$(xy - z)\gamma + (1 - xyz)\zeta$	$D^3$	$(D^2 - D)\gamma + (1 - D^3)\zeta$
$C_{16}^{16}$	$yz^2$	$(xy - z^3)\gamma + (z^2 - xyz)\zeta$	$D$	$(1 - D)(\gamma + \zeta)$
$C_{17}^{16}$	$xy^2z^2$	$(y - xz)\beta$	$D^4$	$(1 - D)\beta$
$C_{18}^{16}$	$x$	$(x - yz)\alpha$	1	$(1 - D)\alpha$
$C_{19}^{16}$	$xy^2$	$(y - x^3z)\alpha$	$D^2$	$(1 - D^3)\alpha$
$C_{20}^{16}$	$xy^2$	$(y - x^3z)\alpha + (x^2z - xy)\zeta$	$D^2$	$(1 - D^3)\alpha + (D^2 - D)\zeta$
$C_{21}^{16}$	$yz^2$	$(xz - y)(\gamma - z\zeta)$	$D^2$	$(D - 1)(\gamma - D\zeta)$
$C_{22}^{16}$	$yz^2$	$(1 - z^2)(\gamma - z\zeta)$	$D^3$	$(1 - D^2)(\gamma - D\zeta)$
$C_{23}^{16}$	$y^2z^2$	$(xz^2 - yz)\gamma + (y - xz^3)\zeta$	$D^3$	$(D^2 - D)\gamma + (1 - D^3)\zeta$
$C_{24}^{16}$	$xyz^3$	$(z^2 - y^2)\alpha$	$D^5$	0
$C_{25}^{16}$	$x^2y$	$(y - xz)\alpha + (z - xy)\zeta$	$D^2$	$(1 - D)(\alpha + \zeta)$
$C_{26}^{16}$	$yz$	$(y - xz^3)\zeta$	$D$	$(1 - D^3)\zeta$
$C_{27}^{16}$	$x$	$(1 - xyz)\zeta$	$D$	$(1 - D^3)\zeta$
$C_{28}^{16}$	$y^3z$	$(y^2 - z^2)\zeta$	$D^4$	0

TABLE II. Decomposition of variables from table I into generators of first generation TDI. Only valid in the approximation of three unequal constant arms. 'Timeshift' denotes the delay to be applied to the combination constructed from the algorithm given in [5], i.e., the factor  $E$  in eq. (9). We also report how these expression further simplify if one assumes all arms to be equal (0th generation TDI), i.e., when assuming  $x = y = z \equiv D$ . Note that some variables cancel exactly under this assumption.



FIG. 3. Secondary noise levels in  $(1 - xyz)C_1^{16}$  compared to the residual between the approximation given in eq. (11b) and the exact expression given in table I. Laser noise is included in the simulation, but fully suppressed by TDI. In addition, we give an analytical estimate of the expected level of the secondary noise levels and we report the 1 pm noise requirement curve as well.

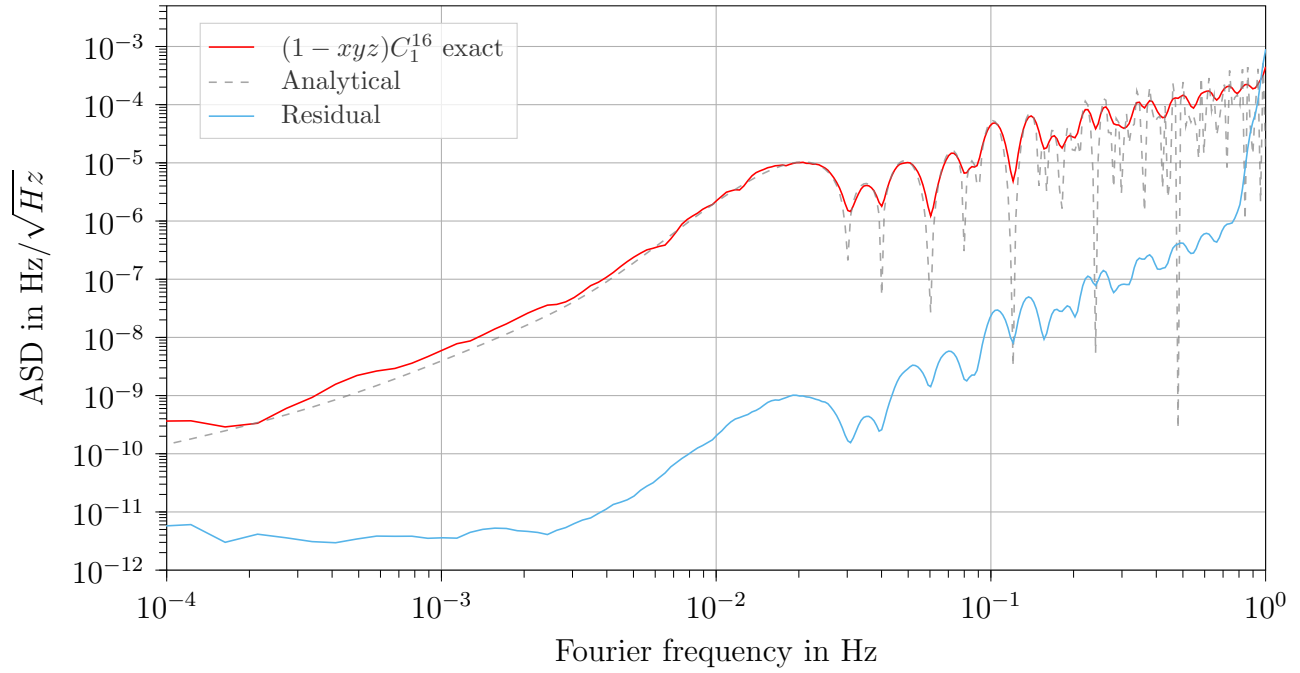
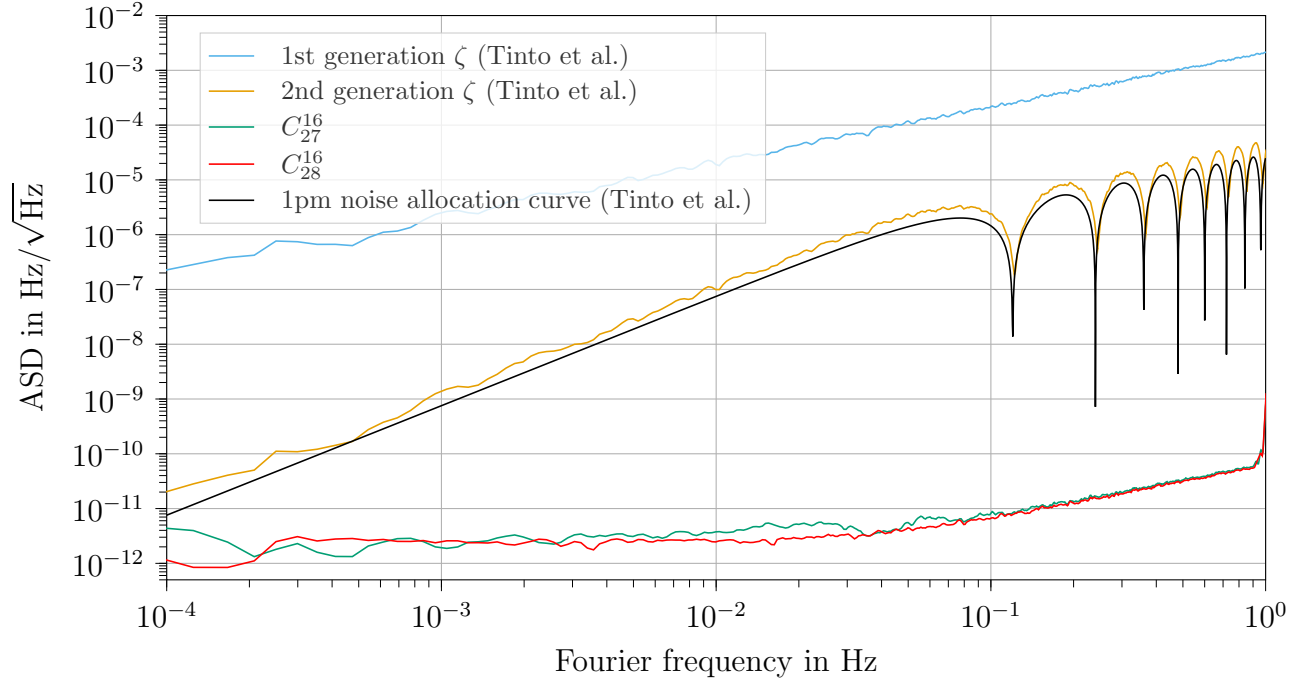


FIG. 4. Laser noise residuals for 1st and 2nd generation  $\zeta$  from the literature compared to  $C_{27}^{16}$ ,  $C_{28}^{16}$  and the 1 pm allocation.  $C_{27}^{16}$  and  $C_{28}^{16}$  perform significantly better than the previously known second generation  $\zeta$ , for which the residual laser noise level is above the 1 pm curve (computed accounting for the TDI transfer function). The residuals we see for  $C_{27}^{16}$  and  $C_{28}^{16}$  are typically explained by numerical noise, the arm-length mismatch, aliasing and interpolation errors [11].



## 4. CONCLUSION

We have shown explicitly how all 34 second generation core TDI combinations up to 16 links presented in the literature can be expressed in terms of the four first-generation variables  $\alpha, \beta, \gamma$  and  $\zeta$ . We also provide the symmetry rules extending these results to all 210 distinct combinations up to 16 links.

We have verified numerically that these expressions are valid to within 3-5 orders of magnitude, such that a set of four second generation versions of  $\alpha, \beta, \gamma$  and  $\zeta$  should be sufficient for the purpose of instrumental noise characterisation.

One possible set are the combinations  $\tilde{\alpha}, \tilde{\beta}, \tilde{\gamma}$  and  $\tilde{\zeta}$ , as introduced in section 3.2. While  $\tilde{\alpha}, \tilde{\beta}$  and  $\tilde{\gamma}$  are already known from the literature,  $\tilde{\zeta}$  (as well as the other variants of  $\zeta$  in table II) is new, and significantly more capable of suppressing laser noise than the second generation  $\zeta$  proposed before [7]. Since the first generation  $\zeta$  is known to be insensitive to GWs at low frequencies, we expect this property to transfer to all its second generation counterparts, making them useful as noise monitors for the LISA mission, as explored in [6].

However, as already discussed in [4–6], other combinations might have practical advantages: some, such as  $C_6^{16}, C_7^{16}, C_8^{16}, C_{21}^{16}$  and  $C_{22}^{16}$ , use just 4 out of the full 6 laser links, such that they are unaffected in case of a loss of one or two inter-satellite links. Others, such as the Michelson-like combinations  $C_1^{16}, C_4^{16}$  and  $C_5^{16}$ , use just 4 inter-satellite links and in addition just 2 constellation arms, thus they remain available in case of a complete failure of one of the LISA arms.

Moreover, as we illustrated in fig. 1, the typical singularities present in the transfer function of all second generation TDI variables appear at different frequencies for the different combinations. This might allow some combinations to be more favourable for detecting signals close to the singular frequencies of other variables.

In particular, another possible set of combinations we found are  $C_{28}^{16}$  and the cyclic permutations of  $C_{24}^{16}$ , for which these singularities appear outside the LISA band. On the other hand, the small delay differences appearing in them might cause numerical instabilities. The next best option in terms of number of in-band zeros would be the set of  $C_2^{12}$ , its cyclic permutations and  $C_3^{12}$ .

Last but not least, combinations with multiple measurements require shorter segments of

data to compute a single data point of the TDI combination. For instance, each of the two beams of  $C_1^{12}$  require summation of the light travel time for 6 consecutive links, or about  $6 \times 8.33 \text{ s} \approx 50 \text{ s}$ . The beams of  $C_2^{12}$ , on the other hand, use only up to 4 links at a time, corresponding to just  $4 \times 8.33 \text{ s} \approx 33 \text{ s}$ .

To conclude, further studies are needed to give a final recommendation which combinations should be used for the data analysis pipeline. In particular, we plan to analyse the sensitivity of these TDI channels with respect to GWs to be able to compute their signal to noise ratio (SNR) and understand what kind of information we can recover through each channel. Moreover, we did not investigate the case of 1.5 generation TDI using 6 generators, as we notice that the 1st generation was enough to accurately reproduce the response of all core TDI variables with respect to instrumental noise. Still, it might be valuable as a follow up study to see if we can extract additional information in this case.

## 5. ACKNOWLEDGEMENT

We thank the LISA Trento group for the fruitful discussion, in particular S. Vitale and D. Vetrugno. We also want to thank M. Staab from the AEI in Hannover for the useful comments on improving this manuscript. M.M thanks the Agenzia Spaziale Italiana and the Laboratorio Nazionale di Fisica Nucleare for supporting this work. O.H. gratefully acknowledges support by the Deutsches Zentrum für Luft- und Raumfahrt (DLR, German Space Agency) with funding from the Federal Ministry for Economic Affairs and Energy based on a resolution of the German Bundestag (Project Ref. No. 500Q1601 and 500Q1801).

## Appendix A: Time shift operators

This paper makes use of time shift operators. They act on time dependent functions by evaluating them at another time. We thus define the following notations related to time-shift operators and TDI combinations:

- Delay operator:  $D_{ij}\phi_j(\tau) = \phi_j(\tau - d_{ij}(\tau))$ .

Given a time of reception  $\tau$  of a beam on spacecraft  $i$ , evaluates the phase  $\phi_j$  of that beam at the time of emission at spacecraft  $j$ , which we write as  $\tau - d_{ij}(\tau)$ . Note that depending on what frame  $\phi_j(\tau)$  is defined in, the computation of  $d_{ij}$  can include a change in reference frames, and clock offsets.

- Advancement operator:  $A_{ij}\phi_j(\tau) = \phi_j(\tau + a_{ij}(\tau))$ .

Given a time of emission  $\tau$  of a beam from spacecraft  $j$ , evaluates the phase  $\phi_j$  of that beam at the time of reception on spacecraft  $i$ , which we write as  $\tau + a_{ij}(\tau)$ . Fulfills  $D_{ij}A_{ji}\phi_i(t) = \phi_i(t)$ .

- Multiple Delay operators:  $D_{ij}D_{jk}\phi_k(\tau) = \phi_k(\tau - d_{ij}(\tau) - d_{jk}(\tau - d_{ij}(\tau)))$ .
- Multiple Delay and Advancement operators:  $A_{ni}D_{ij}D_{jk}\phi_k(\tau) = \phi_k(\tau + a_{ni}(\tau) - d_{ij}(\tau + a_{ni}(\tau)) - d_{jk}(\tau + a_{ni}(\tau) - d_{ij}(\tau + a_{ni}(\tau))))$ .

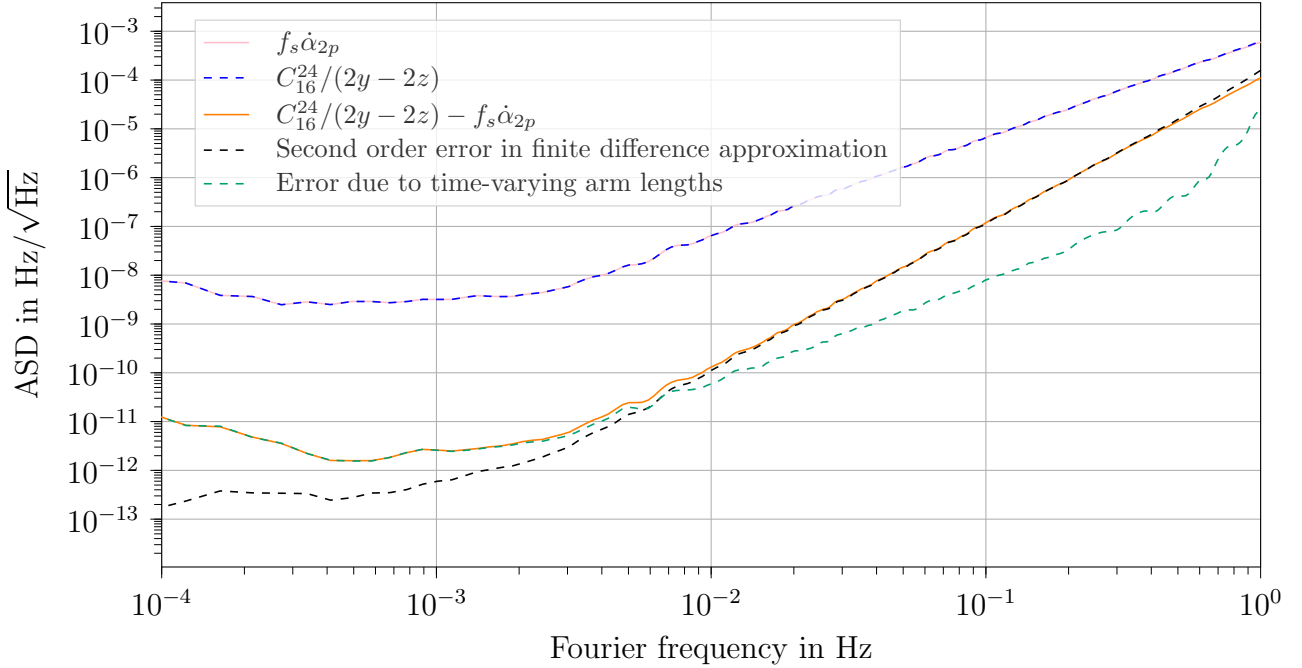
## Appendix B: Numerical approximations of $\dot{\alpha}$

We want here to evaluate how accurately we can approximate the derivative of  $\alpha$ .

Figure 5 shows the comparison between the two point finite difference of  $\alpha$ , which we denote by  $\dot{\alpha}_{2p}$ , and the expression of  $C_{24}^{16}$  reported in table II. The plot shows also the residuals between the two numerical computations and a model which explains their values. While the computations agree within three orders of magnitudes at low frequencies, the error increases towards higher frequencies where the residuals reach about one order of magnitude below the actual value.

This behaviour of the residuals can be explained by two separate effects. For the high frequencies range, we have to take into account the inequality between the time differences,  $\delta$ , we consider to approximate the derivative of  $\alpha$  in  $\dot{\alpha}_{2p}$  and  $C_{24}^{16}$ , respectively.

FIG. 5. Comparison between the estimation of a two-point finite difference derivative of  $\alpha$  and  $C_{24}^{16}$ .



In both cases, we have a finite difference of the form  $\frac{\alpha(t) - \alpha(t - \delta)}{\delta}$  which we can expand to first order in  $\delta$  to get:

$$\frac{\alpha(t) - \alpha(t - \delta)}{\delta} \approx \dot{\alpha}(t) - \frac{\delta}{2} \ddot{\alpha}(t), \quad (\text{B1})$$

where  $\delta = 2(y^d - z^d)$  for  $C_{24}^{16}$  and  $\delta = 1/f_s$  for  $\dot{\alpha}_{2p}$ , while  $f_s = 4$  Hz is the sampling frequency. Thus the difference between the two approximated derivatives will be given by:

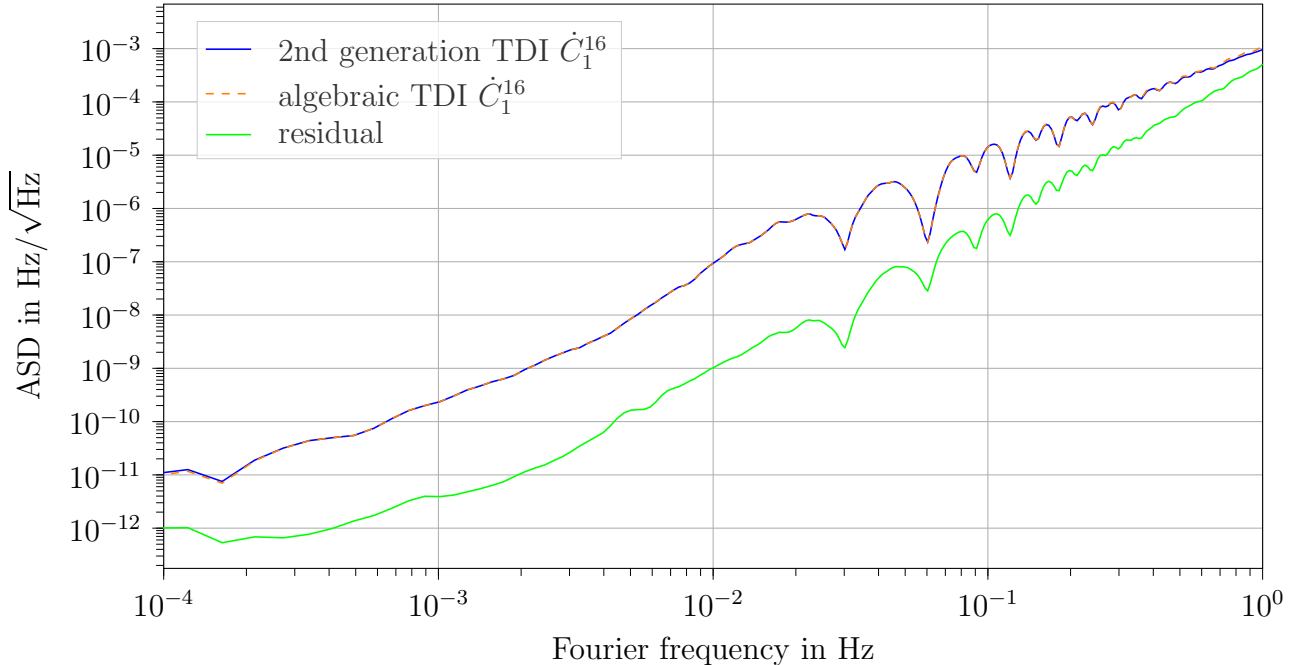
$$\frac{C_{24}^{16}}{2(y^d - z^d)} - f_s \dot{\alpha}_{2p}(t) \approx \left( \frac{1}{2f_s} - y^d + z^d \right) \ddot{\alpha}(t). \quad (\text{B2})$$

In the frequency domain, the additional derivative corresponds to a factor  $2\pi f$ , which explains the increase of the residuals at high Fourier frequencies.

Regarding the low frequencies, the residuals that we see are explained by the error that we make in estimating the  $C_{24}^{16}$  variable out of the TDI  $\alpha$  first generation as visible from fig. 1. We estimate it by rescaling the PSD of  $\dot{\alpha}$  by the ratio between the residual estimated in fig. 1 and the actual PSD of  $C_{24}^{16}$ .

The same reasoning holds for  $\dot{\beta}$ ,  $\dot{\gamma}$  using the cyclic permutations of  $C_{24}^{16}$ , and  $\dot{\zeta}$  using  $C_{28}^{16}$ .

FIG. 6. Comparison between the two-point derivative of the combination  $C_1^{16}$  in table I and the version built out of rescaled versions of  $C_{24}^{16}$ , its cyclic permutations, and  $C_{28}^{16}$ , which represent  $\dot{\alpha}$ ,  $\dot{\gamma}$ ,  $\dot{\beta}$ , and  $\dot{\zeta}$ , respectively.



We can then use these variables in place of  $\alpha$ ,  $\beta$ ,  $\gamma$  and  $\zeta$  to build an approximate version of the derivative of  $C_1^{16}$ , using the expression given in table II. Figure 6 shows the comparison between  $\dot{C}_1^{16}$  computed using a two-point derivative and the version computed using  $C_{24}^{16}$ ,  $\hat{C}_{24}^{16}$ ,  $\hat{\hat{C}}_{24}^{16}$  and  $C_{28}^{16}$ , as well as the relative difference between the two calculations. We can see how the residuals are two orders of magnitude lower than the variable we are trying to compute and that they increase at higher frequencies. This is in accordance to the two complementary models described above.

### Appendix C: Symmetries

In this paper, we study only the core combinations from which other variables can be constructed. We summarize here how to apply these symmetries to the decompositions presented in table II.

### 1. Cyclic permutatation

A cyclic permutation maps the spacecraft indices from  $1 \mapsto 2 \mapsto 3 \mapsto 1$ . This corresponds to the following mappings in table II:

- Map  $\alpha \mapsto \beta \mapsto \gamma \mapsto \alpha$ ,
- Map  $x \mapsto y \mapsto z \mapsto x$ ,
- Leave the fully symmetric  $\zeta$  unchanged.

### 2. Mirror symmetry

A mirror symmetry exchanges the role of two spacecraft, for example  $2 \leftrightarrow 3$ . This corresponds to the following mappings in table II:

- Exchange  $\beta \leftrightarrow \gamma$ ,
- Exchange  $y \leftrightarrow z$ ,
- Flip the sign of all combinations.

Similar rules apply for the reflections involving spacecraft  $1 \leftrightarrow 3$  and  $1 \leftrightarrow 2$ , which leave either  $\beta$  and  $y$  or  $\gamma$  and  $z$  unchanged, respectively.

### 3. Time reversal symmetry

The action of a time reversal of the combination is less obvious than the previous two symmetries. Note that a time reversal is equivalent to one of the other two symmetries for most variables. For the ones were this is not the case ( $C_1^{14}, C_{11}^{16}, C_{15}^{16}, C_{17}^{16}, C_{21}^{16}, C_{22}^{16}, C_{24}^{16}$  and  $C_{28}^{16}$ , cf. [6]), we computed the corresponding expression to verify if these variables bring additional information. It turns out that in the approximations of this paper, a time reversal reduces to one of the other symmetries in most cases, plus an additional overall time shift and sign flip. The exceptions are  $C_{21}^{16}$  and  $C_{22}^{16}$ , whose time reversed versions  $C_{21}^{\text{tr},16}$  and  $C_{22}^{\text{tr},16}$



have the decompositions

$$x^2yzC_{21}^{\text{tr},16} = (y - xz)(z\gamma - \zeta), \quad (\text{C1})$$

$$xz^2C_{22}^{\text{tr},16} = (z^2 - 1)(z\gamma - \zeta). \quad (\text{C2})$$

## REFERENCES

- [1] B. P. Abbott *et al.* (LIGO Scientific Collaboration and Virgo Collaboration), *Phys. Rev. Lett.* **116**, 061102 (2016).
- [2] P. A.-S. et al., “Laser interferometer space antenna,” (2017), arXiv:1702.00786 [astro-ph.IM].
- [3] J. W. Armstrong, F. B. Estabrook, and M. Tinto, *The Astrophysical Journal* **527**, 814 (1999).
- [4] M. Vallisneri, *Phys. Rev.* **D72**, 042003 (2005), [Erratum: *Phys. Rev.* D76,109903(2007)], arXiv:gr-qc/0504145 [gr-qc].
- [5] M. Muratore, D. Vetrugno, and S. Vitale, *Classical and Quantum Gravity* **37**, 185019 (2020).
- [6] M. Muratore, D. Vetrugno, S. Vitale, and O. Hartwig, “Time delay interferometry combinations as instrument noise monitors for lisa,” (2021), arXiv:2108.02738 [gr-qc].
- [7] M. Tinto and S. Dhurandhar, *Living Reviews in Relativity* **24** (2021), 10.1007/s41114-020-00029-6.
- [8] S. V. Dhurandhar, K. R. Nayak, and J.-Y. Vinet, *Phys. Rev. D* **65**, 102002 (2002).
- [9] K. Rajesh Nayak and J. Y. Vinet, (2004), 10.1103/PhysRevD.70.102003.
- [10] M. Muratore, *Time delay interferometry for LISA science and instrument characterization*, Ph.D. thesis, University of Trento (2021).
- [11] O. Hartwig, *Instrumental modelling and noise reduction algorithms for the laser interferometer space antenna*, Ph.D. thesis, Leibniz Universität Hannover (2021).
- [12] M. Tinto and S. V. Dhurandhar, *Living Reviews in Relativity* **8** (2005), 10.12942/lrr-2005-4.
- [13] J.-B. Bayle, *Simulation and Data Analysis for LISA: Instrumental Modeling, Time-Delay Interferometry, Noise-Reduction Performance Study, and Discrimination of Transient Gravitational Signals*, Ph.D. thesis, Université de Paris (2019).
- [14] P. Amaro-Seoane *et al.* (LISA Collaboration), *Laser Interferometer Space Antenna*, Tech. Rep. (ESA, 2017) arXiv.org:1702.00786 [astro-ph].